Human Molecular Genetics, 2014, Vol. 23, No. 3 **706–716**
doi:10.1093/hmg/ddt457
Advance Access published on September 18, 2013

NLRP7 affects trophoblast lineage differentiation, binds to overexpressed YY1 and alters CpG methylation

Sangeetha Mahadevan[1,2,5,†], Shu Wen[2,3,†], Ying-Wooi Wan[2,5], Hsiu-Huei Peng[2,‡], Subhendu Otta[2,¶], Zhandong Liu[2,4,5], Michelina Iacovino[6,§], Elisabeth M. Mahen[6], Michael Kyba[6], Bekim Sadikovic[3,||] and Ignatia B. Van den Veyver[1,2,5,3,*]

[1]Interdepartmental Program in Translational Biology and Molecular Medicine, [2]Department of Obstetrics and Gynecology, [3]Department of Molecular and Human Genetics and [4]Department of Pediatrics (Neurology), Baylor College of Medicine, Houston, TX, USA, [5]Jan and Dan Duncan Neurological Research Institute at Texas Children's Hospital, Houston, TX, USA and [6]Lillehei Heart Institute and Department of Pediatrics, University of Minnesota, Minneapolis, MN, USA

Received April 3, 2013; Revised August 12, 2013; Accepted September 13, 2013

Maternal-effect mutations in *NLRP7* cause rare biparentally inherited hydatidiform moles (BiHMs), abnormal pregnancies containing hypertrophic vesicular trophoblast but no embryo. BiHM trophoblasts display abnormal DNA methylation patterns affecting maternally methylated germline differentially methylated regions (gDMRs), suggesting that NLRP7 plays an important role in reprogramming imprinted gDMRs. How NLRP7—a component of the CATERPILLAR family of proteins involved in innate immunity and apoptosis—causes these specific DNA methylation and trophoblast defects is unknown. Because rodents lack NLRP7, we used human embryonic stem cells to study its function and demonstrate that NLRP7 interacts with YY1, an important chromatin-binding factor. Reduced NLRP7 levels alter DNA methylation and accelerate trophoblast lineage differentiation. NLRP7 thus appears to function in chromatin reprogramming and DNA methylation in the germline or early embryonic development, functions not previously associated with members of the NLRP family.

INTRODUCTION

Autosomal recessive loss-of-function maternal-effect mutations in *NLRP7* (HYDM1, OMIM#231090) (1–4) cause biparental hydatidiform moles (BiHMs), a rare gestational disease characterized by a hyperproliferative vesicular trophoblast and the absence of a developing embryo. Molecular studies on these BiHMs revealed a lack of maternally acquired DNA methylation at germline differentially methylated regions (gDMRs) in the imprinting control centers of some paternally expressed genes, including *PEG3*, *SNRPN* and *KCNQ1OT1* (2,5,6). Where tested, the genes have been found to be aberrantly expressed (7). Interestingly, gDMRs that acquire their methylation during paternal germline transmission, such as the DMR upstream of *H19*, have been found to retain their imprinted methylation status in most studies (2,5), with a few exceptions (6). Only a few such genes have been examined, but thus far, no alterations have been found in repeated sequences, CpG islands of genes on the X chromosome that are subject to X-inactivation, or the methylation status of non-imprinted loci (8). Furthermore, women who carry these pregnancies have normal DNA methylation at imprinted and non-imprinted loci (9), which indicates a maternal effect-driven phenotype. These observations suggest that BiHMs result from a failure to reprogram maternally imprinted gDMR

*To whom correspondence should be addressed at: Department of Obstetrics and Gynecology, One Baylor Plaza, Mailstop BCM610, Baylor College of Medicine, Houston, TX 77030, USA. Tel: +1 8328248125; Fax: +1 8328259354; Email: iveyver@bcm.edu
†The authors wish it to be known that, in their opinion, the first two authors should be regarded as joint First Authors and are listed in alphabetical order.
‡Present address: Department of Obstetrics and Gynecology, Chang Gung Memorial Hospital, Chang Gung University, Tao-Yuan, 333, Taiwan.
¶Present address: Central Institute of Brackishwater Aquaculture, 75 Santhome High Road, RA Puram, Chennai 600028, India.
§Present address: Department of Pediatrics, Harbor-UCLA Medical Center, Torrence, CA, USA.
||Present address: Department of Pathology and Laboratory Medicine, McMaster University, Hamilton, ON, Canada.

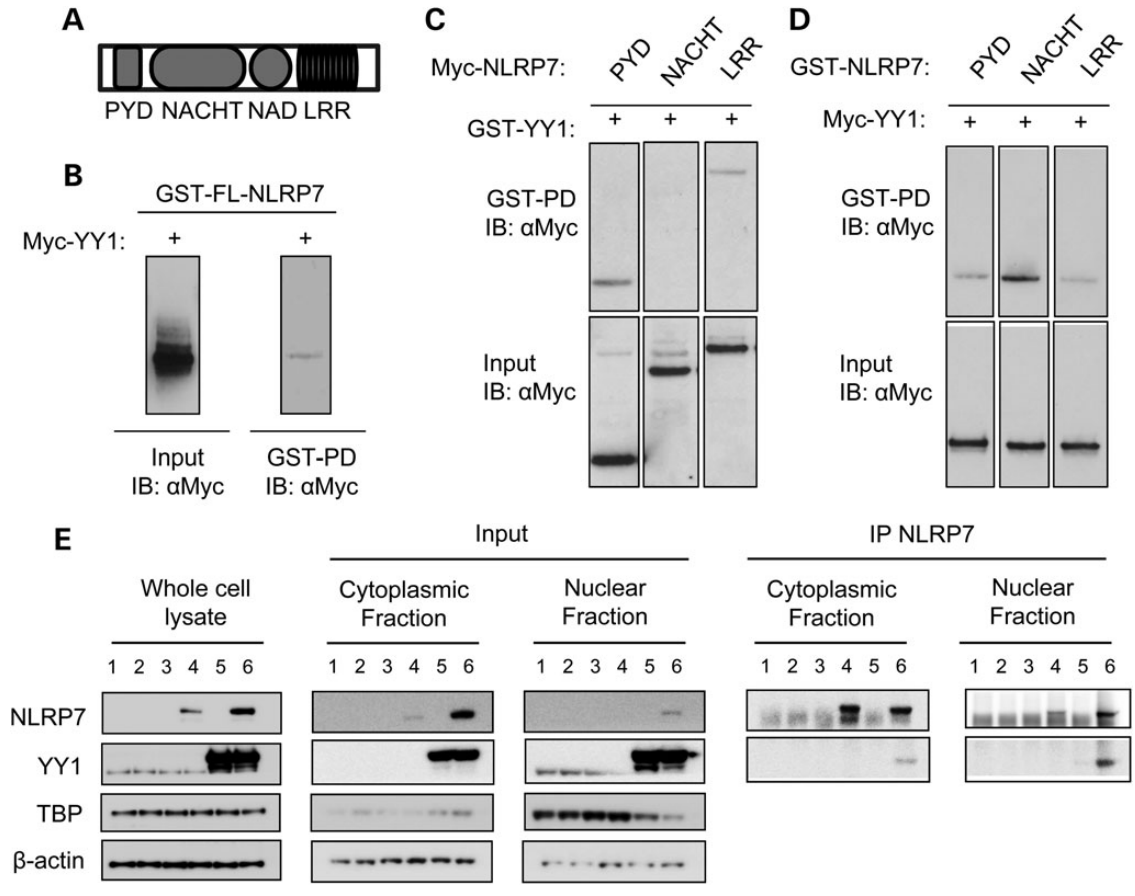

Figure 1. NLRP7 binds to YY1 in both nuclear and cytoplasmic fractions. (**A**) Map of the NLRP7 protein with different domains (PYD: pyrin domain; NACHT: nucleoside-triphosphatase domain named after proteins NAIP, CIITA, HET-E and TP1; NAD: NACHT-associated domain; LRR: leucine-rich repeat). (**B**) GST-tagged full-length NLRP7 (GST-FL-NLRP7) was co-expressed with Myc-tagged YY1. Immunoblotting was performed with an anti-myc antibody (αMyc) on the cell lysate (WB) on input and after pull-down on glutathione-sepharose (GST-PD). (**C**) Myc-tagged NLRP7 PYD, NACHT domain (NACHT) and LRR domain (LRR) were co-expressed with GST-tagged YY1 (GST-YY1 '+' lanes) in HEK293T cells and pulled down with GST-PD. Precipitated material (top panel) or cell lysate (bottom panel; input) was immunoblotted with anti-Myc; the bottom panel shows the western analysis of unprecipitated cell lysates to confirm protein expression in each lane. (**D**) Same experiment as (C) but with tags reversed: NLRP7 domains are GST-tagged and YY1 is Myc-tagged. YY1 binds to the LRR, NACHT and PYD domain. (**E**) HEK293 cells were transfected with transfection agent alone (1), pDESTV5 (2), pDESTmyc (3), NLRP7-V5 (4), myc-YY1 (5) and NLRP7-V5 together with myc-YY1 (6). Whole-cell lysates show appropriate expression in all experimental groups (left panel). Endogenous YY1 (lanes 1–4) is at a lower molecular weight than myc-tagged YY1 (lanes 5 and 6). Subcellular fractionation followed by loading of 10% input from the IP experiment reveals presence of NLRP7 in cytoplasmic (lane 4) as well as nuclear fraction (lane 6). Additionally, there is no endogenous YY1 in the cytoplasmic fraction (lanes 1–4) suggesting an entirely nuclear localization of YY1 (middle panel). IP of NLRP7 followed by blotting with YY1 reveals an interaction of the two proteins in the cytoplasmic and nuclear fractions (right panels).

methylation and that understanding the molecular pathogenesis of BiHMs will provide insight into fundamental mechanisms of genomic imprinting. While several mechanisms to elucidate how gDMRs within the developing oocyte are selected for targeted methylation have been proposed, the specific processes that govern this remain unknown (10–13).

NLRP7 encodes the NOD-like receptor pyrin domain (PYD)-containing 7 protein, which belongs to the CATERPILLER family of proteins, many of which are inflammasome components with roles in innate immunity, inflammation and apoptosis and contain several conserved domains (14–16) (Fig. 1A). The molecular mechanisms by which loss of function of *NLRP7* causes women to have recurrent BiHMs are unclear. Although immune dysfunction in women with *NLRP7* mutations has been proposed to contribute to BiHM formation (17–20), there is to date no evidence that this causes defective reprogramming of maternally acquired DNA methylation and consequently BiHMs. Furthermore, a maternal-effect mutation in *NLRP2*, which is highly homologous to *NLRP7*, is associated with Beckwith–Wiedemann syndrome (BWS) in offspring, who have hypomethylation *in trans* at KvDMR1 in the BWS region and also at the *PEG1* DMR (21,22). *NLRP7*, *NLRP2* and some other *NLRP*s are also highly expressed in human oocytes and early embryos (15,16,23,24).

Owing to the specificity of the defect observed in BiHM concepti and the high expression of NLRP7 in oocytes and the early embryo, we hypothesized that NLRP7 is important for distinguishing which gDMRs should be targeted for DNA methylation in oocytes, or for the acquisition and maintenance of DNA methylation itself at these gDMRs. To this end, we sought to determine whether NLRP7 interacts with specific candidate proteins known to play a role in the imprinting process and whether it affects DNA methylation in human embryonic stem cell (hESC) cultures. The ability to induce trophoblast lineage

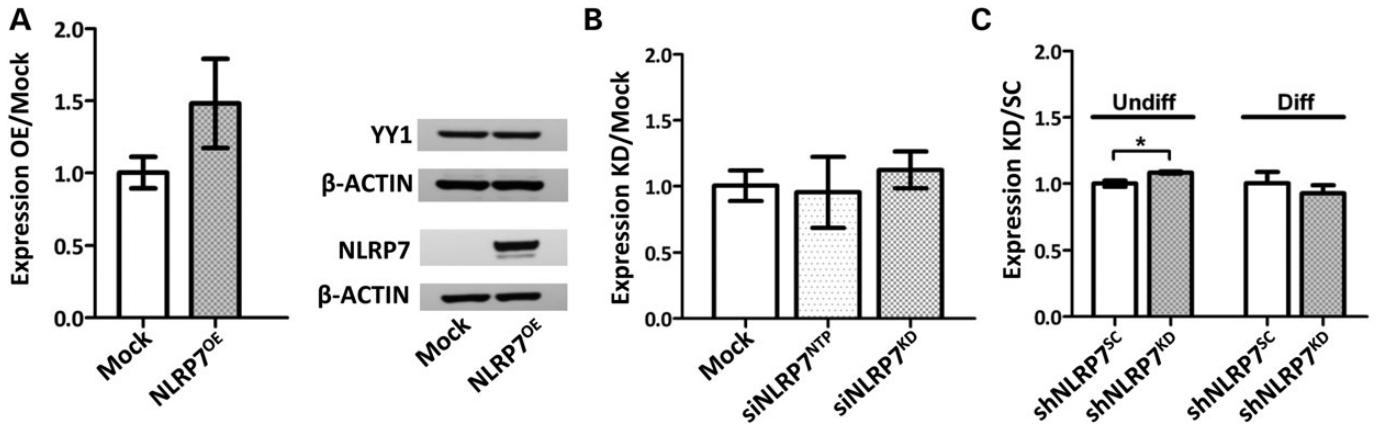

Figure 2. NLRP7 levels do not alter YY1 levels. (**A**–**C**) Expression levels of *YY1* mRNA by RT-qPCR in HEK293T (A), BeWo (B) and H9 hESCs (C) and of protein levels in HEK293T cells (A) with NLRP7 overexpression (A) or knockdown (B and C) are unchanged, except for a marginally significant increased expression in undifferentiated hESCs ($^*P \leq 0.05$).

differentiation with BMP4 in hESCs also allowed us to examine how lack of NLRP7 affects trophoblast differentiation, a process that likely underlies the pathogenesis of the disease.

RESULTS

NLRP7 binds to YY1

We first asked whether NLRP7 interacts with proteins that play a role in chromatin modifications or DNA methylation acquisition and maintenance. We found that glutathione-*S*-transferase (GST)-tagged *NLRP7* expressed in HEK293T cells pulls down myc-tagged Ying-yang 1 (YY1) (Fig. 1B), a factor that can bind to imprinted DMRs in a methylation-dependent manner to alter imprinted gene expression (25), and confirmed the YY1-NLRP7 interaction by co-immunoprecipitation (co-IP) of V5-NLRP7 with myc-YY1 (Supplementary Material, Fig. S1). YY1 binds to the PYD and LRR domains of NLRP7 (Fig. 1C); these binding patterns were confirmed when the tags were reversed (Fig. 1D). Thus, transiently overexpressed NLRP7 binds to YY1 via its LRR and PYD domains. Because endogenous expression of *NLRP7* is very low in HEK293T cells (Supplementary Material, Fig. S2), we could not verify these findings *in situ* or with endogenously expressed proteins. To determine the subcellular compartments in which YY1 and NLRP7 interact, we co-transfected HEK293 cells with V5-tagged NLRP7 and Myc-tagged YY1 and compared their interactions in whole-cell lysates, and in nuclear and cytoplasmic fractions to appropriate controls, including transfection agent alone, pDESTV5, pDESTmyc and each tagged protein alone. We found that NLRP7 resides in the cytoplasm and in the nucleus and confirmed that YY1 is a mostly nuclear protein (Fig. 1E). IP of NLRP7 followed by immunoblotting with YY1 revealed interaction of the two proteins in the cytoplasmic and nuclear fractions (Fig. 1E), suggesting that at least part of the interaction occurs in the nucleus. We next attempted to verify binding of endogenously expressed NLRP7 and YY1 by performing co-IP in two cell lines (BeWo trophoblast cells and hESCs) with higher mRNA levels of *NLRP7* with antibodies raised to these proteins. However, despite higher levels of mRNA in both cell types, we could not detect sufficiently high protein levels in western blot analysis with currently available antibodies to NLRP7 or after reciprocal immunoprecipitation experiments (data not shown).

The influence of NLRP7 overexpression on YY1 levels and binding to imprinted gDMRs

We next explored whether the observed interaction between NLRP7 and YY1 affects YY1's expression levels and binding to its recognition sites at imprinted gDMRs of *PEG3* and *SNRPN*, which normally acquire methylation in the maternal germline. We first showed that overexpression of NLRP7 did not alter mRNA and protein expression levels of YY1 (Fig. 2A). We then performed chromatin-immunoprecipitation (ChIP) with anti-YY1 in HEK293T cells that transiently overexpress *NLRP7* ($NLRP7^{OE}$), followed by real-time quantitative PCR (qRT-PCR) amplification of known YY1-binding sites at the gDMRs of *PEG3* and *SNRPN*, at sites flanking these regions and at non-imprinted YY1-binding sites. We did not find a significant change in the binding of YY1 at any of these regions (data not shown). Since these experiments were performed with overexpressed *NLRP7* in a cell line with low endogenous *NLRP7* expression (Supplementary Material, Fig. S2), we also investigated whether reducing its levels affects DNA-binding of YY1 to gDMRs. We transfected BeWo cells, a commonly used trophoblast cell line with high endogenous *NLRP7* expression (Supplementary Material, Fig. S2), with a mixture of siRNAs that target *NLRP7* to reduce *NLRP7* mRNA levels by 85% (Supplementary Material, Fig. S3A) without affecting expression of the homologous *NLRP2* gene (Supplementary Material, Fig. S3B). As expected, *NLRP7* knockdown ($siNLRP7^{KD}$), similar to overexpression of *NLRP7*, did not affect expression of *YY1* (Fig. 2B). We also did not see changes in its binding to the gDMRs of *PEG3* and *SNRPN* compared with mock-transfected BeWo cells or cells transfected with the negative control non-targeting siRNA pool ($siNLRP7^{NTP}$).

Modeling loss of NLRP7 in hESCs

The absence of *NLRP7* from the rodent genome (15) precludes generation of mouse models for BiHMs. Instead, to investigate whether NLRP7 and its effect on YY1 function influence

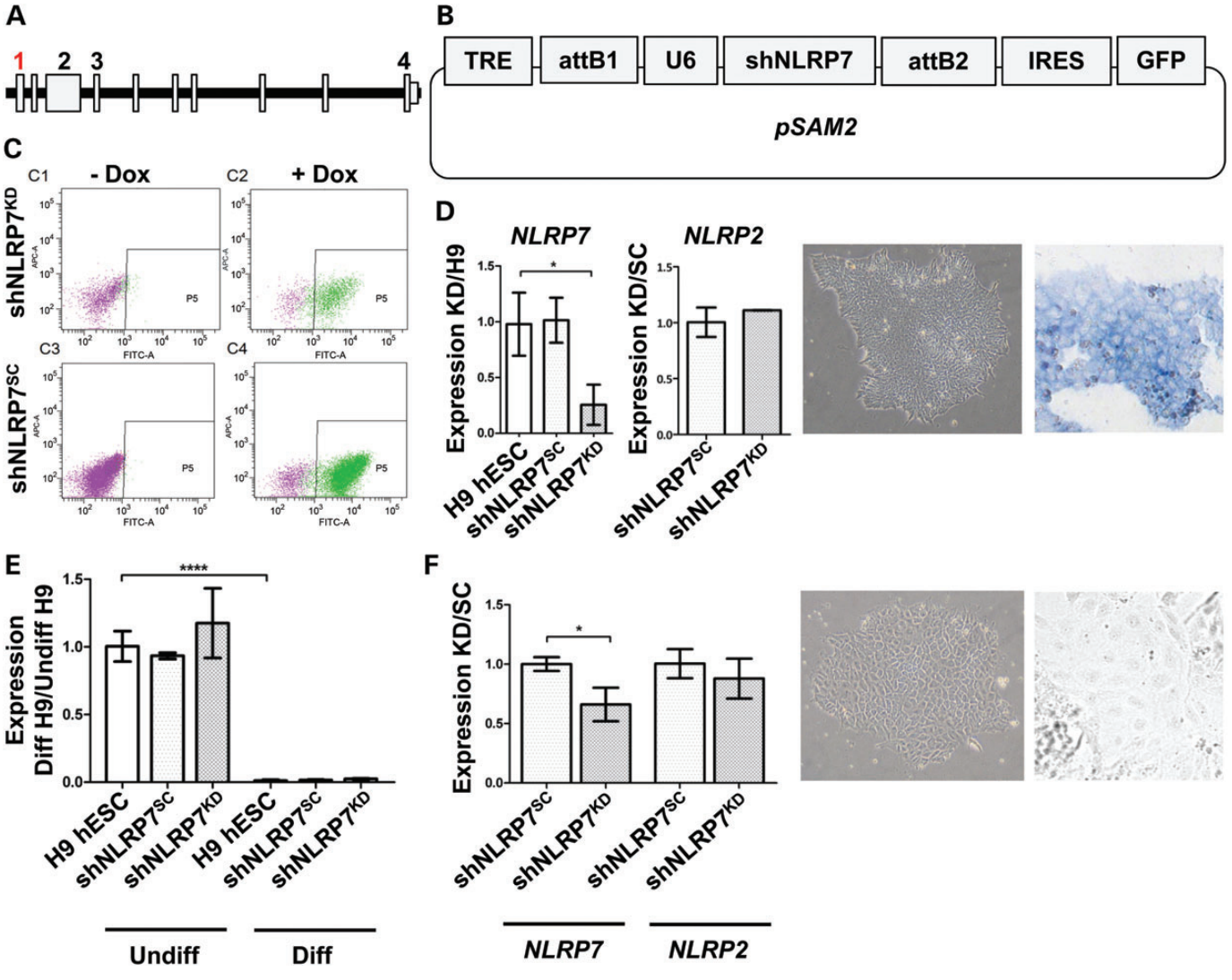

Figure 3. *NLRP7* knockdown in H9 cells. (**A**) Genomic region with exons of NLRP7. Position of shRNA sequences is indicated by numbers 1–4; number 1 (in red) was used for knockdown in hES cells. (**B**) Map of the pSAM2 vector containing the *NLRP7* shRNA sequence (*shNLRP7*). Constitutive expression of the *NLRP7* knockdown cassette is controlled by a U6 RNA promoter. The GFP cassette is separated from the shNLRP7 cassette by an IRES sequence and controlled by a doxycycline-inducible promoter (TRE, tetracycline response element; GFP, green fluorescent protein; IRES, internal ribosomal entry site; attB1 and attB2, cloning sites for Gateway® cloning; U6, U6 promoter sequence for constitutive shRNA expression). (**C**) FACS results of hES cells transduced with the *pSAM2* vector containing the *shNRLP7* (upper panels; $shNLRP7^{KD}$) and the vector containing the scrambled *shRNA* (lower panels; $shNLRP7^{SC}$). C1 and C3 show the absence of GFP-labeled cells without doxycycline induction, and C2 and C4 show the presence of GFP-positive cells in gate P5 after doxycycline induction. GFP-positive cells were triple-sorted for purification. (**D**) *NLRP7* mRNA expression (left graph) is reduced by 80% in $shNLRP7^{KD}$ hESCs that express $shNLRP7^{KD}$ compared with untransduced cells (H9 hESCs) and cells containing the scrambled $shNLRP7^{SC}$ ($^{*}P \leq 0.05$), but *NLRP2* expression (right graph) is unaffected. $shNLRP7^{KD}$ hESCs exhibit characteristic pluripotent colony morphology within 24 h of culture and high alkaline phosphatase (blue stain) activity prior to differentiation. (**E**) qRT-PCR results show significant reduction of *POU5F1* mRNA expression to undetectable levels after 7 days of BMP4-induction of differentiation ($^{****}P \leq 0.0001$). (**F**) *NLRP7* mRNA expression remains reduced by ~50% after differentiation in $NLRP7^{KD}$ hESCs (left graph) that express $shNLRP7^{KD}$ compared with cells expressing scrambled $shNLRP7^{SC}$ (sh$NLRP7^{SC}$) ($^{*}P \leq 0.05$), but *NLRP2* expression (right graph) remains unaffected. Morphological changes after 24 h of BMP4-induced differentiation: hESCs adopt a more cuboidal shape. Alkaline phosphatase activity (blue stain) disappears after 7 days of differentiation with BMP4 when cells also adopt the larger, flatter more trophoblast-cell-like shape.

trophoblast differentiation, we studied hESCs, which have relatively high *NLRP7* expression (Supplementary Material, Fig. S2) and can be induced by BMP4 to differentiate along trophoblast lineages (26). We used a retrovirus-based *pSAM2* vector (27,28) to stably express a short hairpin (sh) RNA ($shNLRP7^{KD}$) that targets a different NLRP7 region than the siRNA pool used in BeWo cells (Fig. 3A–C). This reduced *NLRP7* in hESCs by ~80% without affecting *NLRP2* expression (Fig. 3D). Despite reduced *NLRP7* expression, the cells maintained their normal undifferentiated morphology and alkaline phosphatase expression, suggesting that NLRP7 is not necessary for hESC self-renewal or maintenance (Fig. 3D). We also observed no effect on YY1 expression levels (Fig. 2C).

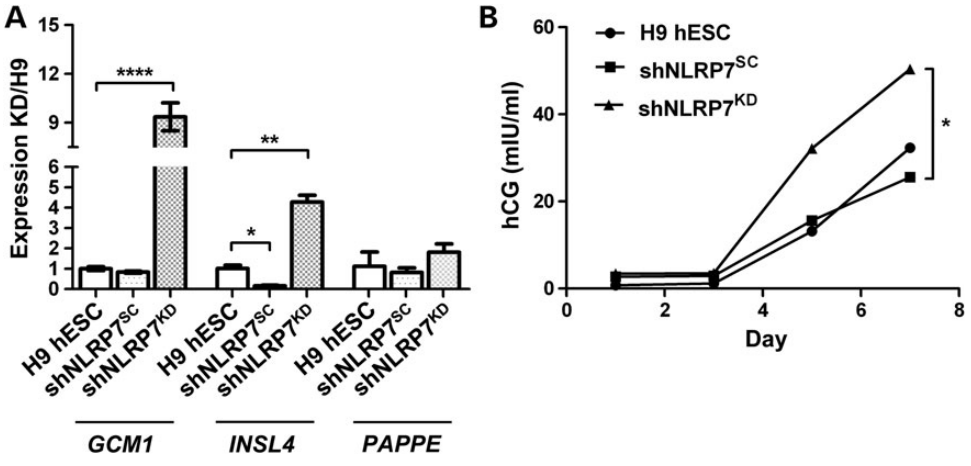

Figure 4. *NLRP7* knockdown promotes trophoblast differentiation in hES cells. (**A**) qRT-PCR of trophoblast lineage markers after 7 days of BMP4-induced differentiation in $shNLRP7^{KD}$ cells, compared with untransduced cells (H9 hESCs), and cells expressing the scrambled shRNA ($shNLRP7^{SC}$) showed high expression of *GCM1* ($^{****}P \leq 0.0001$) and *INSL4* ($^{**}P \leq 0.01$), but no change in *PAPPE* expression. (**B**) Quantification by ELISA at 1, 3, 5 and 7 days of BMP4-induced differentiation of hCG secreted in the culture medium: levels increase by day 5 in all three lines, but are higher at both day 5 and day 7 in $shNLRP7^{KD}$ cells, compared with $shNLRP7^{SC}$ cells and untransduced H9 ESCs.

Reduced levels of NLRP7 accelerate trophoblast differentiation of hESCs

Adding BMP4 to the hESC cultures induced trophoblast lineage differentiation as evidenced by loss of expression of pluripotency marker *POU5F1* (Fig. 3E), morphological changes and loss of alkaline phosphatase activity (Fig. 3F). Differentiated $shNLRP7^{KD}$ cells maintained 50% reduced *NLRP7* expression without alterations in *NLRP2* expression (Fig. 3F). Expression of trophoblast markers *GCM1* and *INSL4*, but not *PAPPE*, was significantly increased in $shNLRP7^{KD}$ cells 7 days after the induction of differentiation (Fig. 4A). Furthermore, the amount of human chorionic gonadotropin (hCG) secreted in the media increased by day 5 in all hESC cultures, but levels were significantly higher in $shNLRP7^{KD}$ hESC cultures than in $shNLRP7^{SC}$ or untransduced hESCs (Fig. 4B). These findings are striking, considering that molar pregnancies are characterized by excessive trophoblast proliferation and high hCG production.

Altered methylation of CpG islands in $shNLRP7^{KD}$ hESCs

Although hESCs do not completely recapitulate the epigenetic states of germ cells or embryos and have relatively stable epigenetic marks at imprinted genes, they can yield useful data on molecular mechanisms that underlie chromatin modifications and DNA methylation in undifferentiated and differentiated states (29,30). Considering recent data supporting widespread gDMR methylation reprogramming in mouse female germ cells (31–33), we reasoned that DNA methylation profiling of $shNLRP7^{KD}$ hESCs could uncover a subset of the CpGs that require NLRP7 for normal methylation. We hybridized three replicates each of undifferentiated and differentiated $shNLRP7^{KD}$, $shNLRP7^{SC}$ and untransduced hESCs to a HumanMethylation450 BeadChip array and analyzed the data using the following filters: ANOVA *P*-value, mean methylation difference and *F*-value (indicating signal-to-noise ratio) in three consecutive probes within a single region. As shown in the volcano plot (Fig. 5A) and Supplementary Material, Table S1, we found significantly altered DNA methylation at 864 probes (0.18% of all probes on the array) in $shNLRP7^{KD}$ cells at a signal-to-noise ratio of $F > 50$, with more hypermethylation (788 probes) than hypomethylation (76 probes), the majority of which are in CpG islands (Supplementary Material, Table S2). There were 234 distinct genes with altered methylation at $F > 5$ (Supplementary Material, Table S3).

To follow up on the observed interactions between YY1 and NLRP7, we next searched for loci that had altered methylation patterns at YY1-binding sites by first overlapping sequences within 5 kb of probes on the array with those of the 11 608 YY1-bound sites identified by ChIP-Seq on hESCs [Gene Expression Omnibus (GEO) ID: GSM803513]. This revealed potential YY1-binding sites for 11 201 of the 21 242 genes represented on the array. We overlapped this list with the 234 genes with most significantly altered methylation (Supplementary Material, Table S3) and found 15 genes in common (Fig. 5B), of which several also had the greatest methylation changes (Supplementary Material, Table S3), supporting a functional connection between YY1 binding and DNA methylation. We selected three loci for the validation of hypermethylation in differentiated (Fig. 5C and D) and undifferentiated (Supplementary Material, Fig. S4) hESCs. We chose *SUCLG2* because it showed the most significant change in methylation. *FBXO4* was of interest because it is a 'reprogramming DMR' in human iPS cells resistant to general demethylation during reprogramming (34). *ZFP42* is a pluripotency marker specific to the eutherian lineage thought to have arisen through a duplication of the ancestral *YY1* gene (35). *ZFP42* is highly expressed in undifferentiated ESCs, where it interacts with POU5F1, NANOG and SOX2 (36,37), and loss of its murine ortholog, *Rex1*, causes hypermethylation in blastocysts at DMRs of maternally imprinted genes, *Peg3* and *Gnas* (38). Hypermethylation of *FBXO4* and *ZFP42* was associated with decreased expression (Fig. 5E).

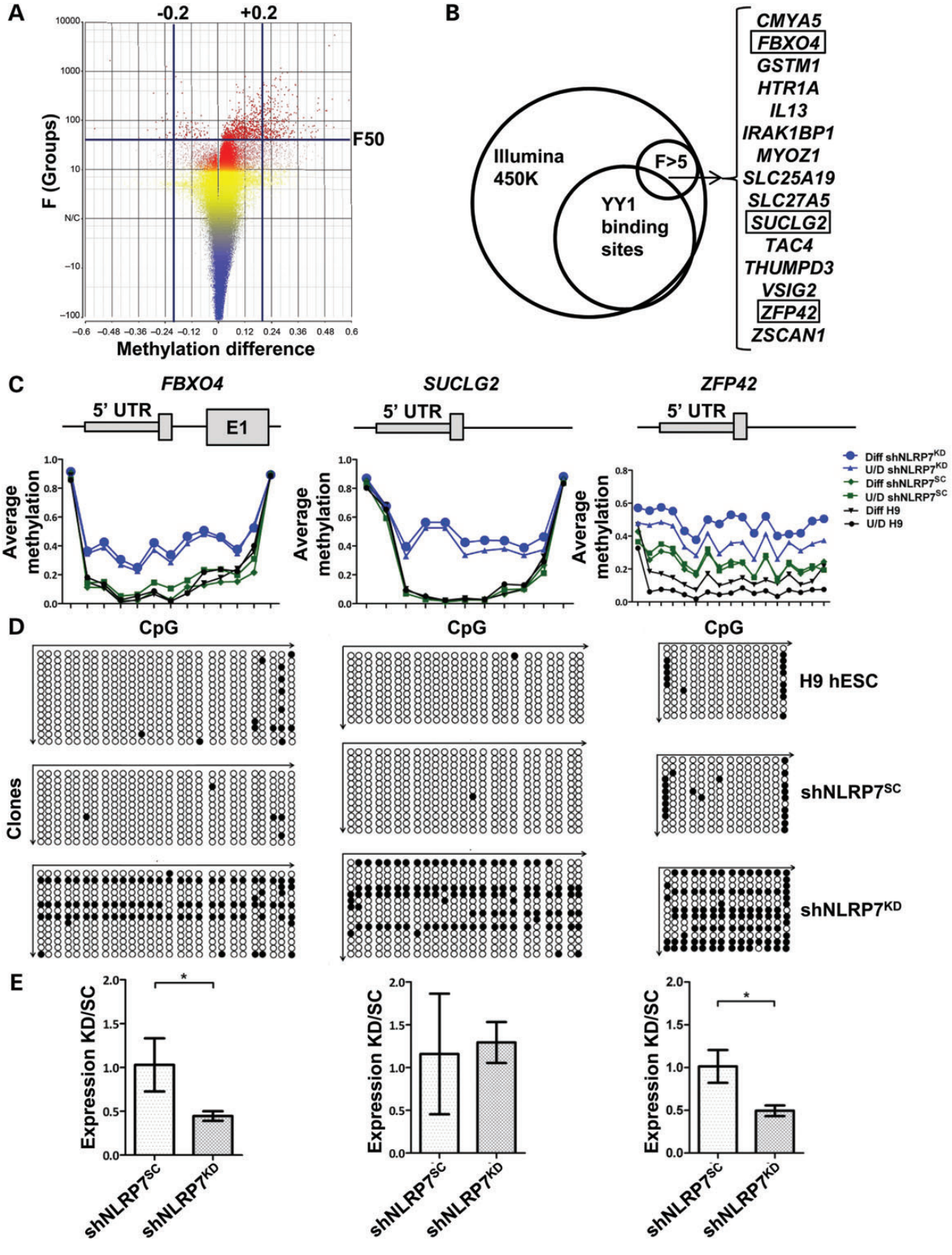

Because BiHM pregnancies caused by maternal-effect mutations in *NLRP7* show loss of methylation at maternally imprinted gDMRs, we also searched for DNA methylation changes of probes within 5 kb of known imprinted gDMRs upon knockdown of *NLRP7* by overlapping them with lists of imprinted genes (www.geneimprint.com and igc.otago.ac.nz), but not surprisingly considering the epigenetic state of hESCs (29,30), we did not see any significant changes in the *shNLRP7^{KD}* cells (Supplementary Material, Fig. S5). We also did not find any changes in DNA methylation at *ZFP42* in HM compared with term placenta, and maternal leukocyte-derived DNA (Supplementary Material, Fig. S6). These observations, together with the fact that the *FBXO4* iPS methylation resistant-reprogramming DMR (34) has altered methylation in hESCs, have important implications for understanding the function of NLRP7 in reprogramming: it suggests that the consequences of NLRP7 inactivation on methylation of CpG sites and gene expression may not be limited to imprinted DMRs, but may be more widespread.

DISCUSSION

Two key features of BiHMs, the lack of methylation at maternally imprinted (methylated) gDMRs and the hyperplastic vesicular trophoblast with no normal embryonic development, point toward an important role of NLRP7 in germ cells and early development. In support of this prediction, our data demonstrate that NLRP7 interacts with the important chromatin regulator YY1. We found that its knockdown in hESCs has a widespread impact on DNA methylation and trophoblast differentiation.

Differential CpG methylation at gDMRs is the most widely studied imprinting mark, and controls mono-allelic expression of single or clustered imprinted genes. In addition to DNA methylation, histone modifications and DNA-binding proteins have been implicated in the establishment and read-out of imprinting marks. Among the studied DNA-binding proteins, YY1 can bind to imprinted gDMRs in a methylation-dependent manner to help coordinate imprinted gene expression (25). It remains unclear whether NLRP7 participates directly in the binding of YY1 to DNA or can affect YY1's affinity for DNA through another mechanism.

All members of the NLRP family of proteins were until now considered to be cytoplasmic components of the inflammasome with a role in innate immunity and apoptosis (39,40). Although NLRP7 had not been previously shown to localize to the nucleus (23), we found that NLRP7, when overexpressed, can be found in the nucleus and can interact with YY1 in both the nuclear and cytoplasmic compartments. We speculate that low endogenous protein levels have thus far prevented detecting the presence of a small fraction of the total cellular NLRP7 within the nucleus. Furthermore, the process of germline reprogramming of maternal imprinting marks occurs in the growing oocyte during prophase I of meiosis, which arrests at diplotene stage until the time of ovulation when meiosis resumes and the nuclear envelope disappears (32,41). It is thus possible that persistence of maternally transcribed genes such as *NLRP7* and *NLRP2* is required to protect imprinting marks at gDMRs once meiotic division progresses, which is consistent with the imprinting disease phenotypes caused by maternal-effect mutations in these genes and with their expression patterns (1–3,21). We speculate that rodents, which have shorter intervals between early embryonic development and reproductive maturity, can achieve this with a single gene (*Nlrp2*), whereas the longer mammalian intervals between early development and reproductive maturity benefit from the evolutionary duplication event that generated *NLRP7* from this single ancestral gene. This is consistent with the recent discovery that maternal-effect mutations in *KHDC3L*, which is likewise not present in rodents, also cause BiHMs (42).

We examined the function of NLRP7 in hESCs for three important reasons. First, because there is no rodent *NLRP7* ortholog, *in vivo* studies in an animal model are not possible. Second, hESCs are pluripotent cells that can be differentiated into trophoblast lineages (26,43), the primary diseased tissue in BiHMs. Third, although hESCs are derived from the inner cell mass at a stage when imprinted loci have relatively stable epigenetic marks (30,44), and thus do not fully recapitulate the epigenetic states of germ cells (and only partially those of developing pre-implantation embryos), they can yield useful data on molecular mechanisms that underlie differences in chromatin states between undifferentiated and differentiated cells (44). The enhanced differentiation of hESCs into trophoblast-like lineage upon NLRP7 knockdown is remarkable, given that maternal deficiency of NLRP7 causes pregnancies to develop into hydatidiform moles, characterized by hyperplastic vesicular trophoblast development and production of high levels of hCG. It validates hESCs as the best available model to study the mechanisms by which maternal inactivation of NLRP7 causes BiHMs.

Another intriguing finding was that DNA methylation changed significantly with the knockdown of NLRP7 at multiple loci that were different from those with altered methylation because of induced differentiation. Although initially surprising, the absence of DNA methylation changes at imprinted gDMRs upon NLRP7 knockdown can be explained by the previously reported high degree of epigenetic stability and resistance to perturbation at imprinted loci in hESC lines (30). Nevertheless, the combined observations that NLRP7 affects methylation at imprinted loci in the human disorder (BiHMs) and at non-imprinted loci in this study are in line with new data in mice

Figure 5. *NLRP7* knockdown in hES cells alters DNA methylation at multiple loci. (**A**) Volcano plot of methylation data shows methylation difference (*X*-axis) by *F*-value (*Y*-axis). (**B**) Overlap of 11 608 sites bound by YY1 in reported H1 hESC ChIP-seq data with the significantly altered probes from the $F > 5$ list of loci yielded 15 significant loci; loci that were verified are boxed. (**C**) DNA methylation levels at the CpG islands of the *FBXO4* gene (left), *SUCGL2* gene (middle) and *ZFP42* gene (right) are increased in *shNLRP7^{KD}* hESCs. Each is shown as a graph, with methylation levels on the *Y*-axis and the individual probes in the region on the *X*-axis. The partial gene structure is aligned above each graph relative to the distribution of the probes on the graphs. (**D**) Bisulfite sequencing at each of these CpG islands in differentiated untransduced (top), *shNLRP7^{SC}*-transduced (middle) and *shNLRP7^{KD}*-transduced (lower) H9 hESCs confirms the methylation gain upon *shNLRP7^{KD}*. Each horizontal line represents a sequenced clone, open circles represent unmethylated CpG sites and closed circles represent methylated CpG sites. (**E**) Increased methylation correlates with decreased mRNA expression by qRT-PCR in *shNLRP7^{KD}* H9 hESCs compared with *shNLRP7^{SC}* H9 hESCs for *FBXO4* (left) and *ZFP42* (right), but not in *SUCLG2*.

which indicate that hundreds of germline DMRs become methylated in growing oocytes (31–33), but that the majority are transiently imprinted gDMRs—only those that are protected from acquiring methylation on the paternally inherited allele in the early embryo become permanently imprinted gDMRs (33). It remains to be seen whether this requires interaction with YY1 and whether downregulation of ZFP42 contributes to this process.

In conclusion, we show that NLRP7, an NLRP protein with high expression in germ cells, has unanticipated important non-inflammasome functions affecting DNA methylation. This has wider implications for the function of other NLRP family members, especially those that are expressed at early developmental stages (24).

MATERIALS AND METHODS

Cell culture

HEK293T cells and BeWo cells were from American Type Culture Collection and cultured in DMEM supplemented with 10% FBS and antibiotics at 37°C and 5% CO_2 to 80% confluence. H9 hESCs were obtained from the Baylor College of Medicine (BCM) Stem Cells and Regenerative Medicine Center (StaR) stem cell core and maintained in mTeSR1 medium (Stemcell Technologies) in six-well matrigel-coated plates (BD Biosciences). For differentiation into trophoblast, 100 ng/ml recombinant human BMP4 (R&D Systems, 314BP) was added daily to standardized volumes of fresh culture medium for 7 days starting 24 h after seeding the cells at ∼30% confluence. Spent media was collected daily and stored at −80°C for hormone assays. At days 1, 3, 5 and 7 after the initiation of differentiation, hCG levels in the media were quantified by ELISA (AxSYM Total hCG kit from Abbott). Cells were harvested for analysis on day 7.

Transient transfections, co-affinity purification assays

cDNA clones for full-length *NLRP7* (transcript variant 3; NM_001127255.1) and tested candidate interactors were obtained from Open Biosystems (Thermo Scientific Molecular Biology). They were first cloned into pDONR223 and then shuttled by Gateway® cloning (Invitrogen) into mammalian expression vectors 5′-pDESTMyc (gift from Dr Marc Vidal, Dana Farber Cancer Institute) and 5′-GST-pDEST27 (Invitrogen). HEK293T cells were transfected with expression vectors using Lipofectamine 2000 (Invitrogen) and collected after 48 h for co-affinity purification assays. Protein lysates were prepared in lysis buffer containing 20 mM Tris, 180 mM NaCl, 1 mM EDTA, 0.5% NP-40 and protease inhibitor cocktail complete ULTRA Tablet, Mini, *EASY*pack (Roche Applied Science). Glutathione Sepharose-4B Media (GE Healthcare Life Sciences) was used to perform the GST pull-down as per the manufacturer's protocol. Mouse anti-Myc (EMD Millipore, 05-724; 1:1000 dilution) and horse anti-mouse secondary antibody (Cell Signaling Technologies, 7076S; 1:5000 dilution) were used for western blotting and detection.

Subcellular fractionation and co-IP assays

Gateway®-cloned V5-NLRP7 and Myc-YY1 were overexpressed for 48 h in HEK293T cells, and protein lysates were prepared as described above. Protein A Dynabeads (Life Technologies, 10001D) were conjugated with 5 μg of anti-NLRP7 (Imgenex, IMG-6357A), anti-V5 (Life Technologies, R960-25), anti-YY1 (Santa Cruz Biotechnology, sc-1703X) or rabbit anti-IgG (Abcam, ab46540). Subcellular fractions were prepared using the Active Motif Nuclear Extract Kit (Cat no. 40010). Following preparation of the cytoplasmic fraction, the nuclear pellet was washed twice in cold 1 × PBS containing protease inhibitors to eliminate residual cytoplasmic protein. An amount of 100 μl of cytoplasmic and nuclear extracts were then added to Dynabeads conjugated with anti-NLRP7 antibody and allowed to immunoprecipitate overnight at 4C. Ten microliters (10%) was reserved as input. Following overnight immunoprecipitation, the beads were washed four times in cold lysis buffer. Protein was eluted from the bead by boiling at 100°C with 50 mM glycine, pH 2.8. The immunoprecipitated protein and inputs were run on a 4–12% Bis-Tris gel and then transferred to a nitrocellulose membrane. The inputs and immunoprecipitated blot was probed with anti-YY1 and anti-NLRP7 at a 1:1000 dilution. Beta-actin (ab8227) and TATA-binding protein (sc-273) served as purity controls for the cytoplasmic and nuclear fractions, respectively. Anti-mouse and anti-rabbit secondary antibodies from Cell Signaling Technologies (7076S and 7074S, respectively; 1:5000 dilution) were used for detection with Western Lighting™ Ultra chemiluminescence substrate kit (Perkin Elmer, NEL100001EA) and SuperSignal West Pico Chemiluminescent Substrate (Thermo Scientific, 34077).

NLRP7 knockdown

BeWo cells

At ∼60% confluence, 20 pmol of Dharmacon siRNA ON-TARGETplus SMARTpool NALP7 (old nomenclature for NLRP7) (Thermo Fisher Scientific, L-016890-01-0005), containing a mixture of siRNAs that target exons and the 3′ untranslated region of *NLRP7*, was double-transfected with Lipofectamine RNAiMax (Invitrogen, 13778-075) at baseline and at 24 h. Cells were collected 24 h after the second transfection.

hES cells

Four shRNA oligos, targeting different regions of *NLRP7* (Fig. 3A), and a scrambled oligo (negative control) were first inserted into the BLOCK-iT U6 RNAi Entry Vector according to the manufacturer's protocol (Invitrogen BLOCK-iT™ U6 RNAi Entry Vector Kit, K4945-00). The U6 promoter and sh-oligos were subsequently shuttled into the retrovirus-based *pSAM2* lentiviral vector, containing a doxycycline-inducible GFP cassette to identify transduced cells. The different constructed *pSAM2* vectors were electroporated into H9 hESCs and pulsed with 1 μg/ml of doxycycline for 24 h to induce GFP expression. H9 hESCs expressing rtTA and GFP-positive cells were triple-sorted by fluorescence-activated cell sorting (FACS) after pulsing the cultures with doxycycline to induce GFP expression (Fig. 3C). The hESC line with the most efficient

knockdown was used for further experiments. Sequences of the *NLRP7* sh-oligos are *NLRP7-KD-F* (CAC**CGAAACTGGCA GAAATTCTG**TTCAAGAGA**CAGAATTTCTGCCAGTT TC**TT) and *NLRP7-KD-R* (AAAAAA**GAAACTGGCAG AAATTCTG**TCTCTTGAA**CAGAATTTCTGCCAGTTTC**) (bold indicates nucleotides targeting *NLRP7*). The scrambled sh-oligos have the order of six pairs of dinucleotides (bold, underlined and italic) in the targeting regions reversed so as to no longer target *NLRP7* while maintaining similar GC content. Sequences are *NLRP7-SC-F*: CACC***AG***GAACTGGC***GA***AA ATTC***GT***TTCAAGAGA***AC***GAATTT***TC***GCCAGTT***CT***TT; *NLRP7-SC-R*: AAAAAA***AG***AACTGGC***GA***AAATTC***GT***TC TCTTGAA***AC***GAATTT***TC***GCCAGTT***CT***.

ChIP assay

Biological triplicates of HEK293T cells with NLRP7 overexpression, BeWo cells with transient NLRP7 knockdown and H9 hESCs with stable NLRP7 knockdown were cross-linked with 37% formaldehyde to a final concentration of 1%. ChIP was then performed using the SimpleChIP® Enzymatic Chromatin IP Kit (Cell Signaling, 9003S). Micrococcal nuclease-digested chromatin was further sonicated using Diagenode Bioruptor® with 10 pulses of 20 s on and 30 s off at high power to yield sheared chromatin of 150–900 bp. Ten micrograms of chromatin was used per IP with 5 μg of ChIP-grade anti-YY1 (Santa Cruz Biotechnology, sc-1703X). ChIP-grade normal rabbit IgG #2729 and Histone H3 (D2B12) XP® Rabbit mAb (ChIP formulated) from Cell Signaling Technology were used as negative and positive controls, respectively. Two percent input was reserved for qPCR quantification. qPCR of YY1-binding sites at *PEG3* and *SNRPN* was performed using the PerfeCTa® SYBR® Green FastMix (Quanta Biosciences) on a StepOnePlus real-time instrument (Applied Biosystems). Primers for *PEG3* were 5′-CAAGGAGCGCGGCACTCCAC-3′ and 5′-CATAGGTGT GGGGTTGTCCA-3′ and for *SNRPN* were 5′-TCTCTGTTGG GAACCAGGTC-3′ and 5′-CATCTTGAAGGAGCTGCAC A-3′. Fold-enrichment was calculated by the percent input method.

DNA methylation profiling

Total genomic DNA was prepared using a Gentra Puregene DNA extraction kit (Qiagen) from three biological replicates each of $shNLRP7^{KD}$, $shNLRP7^{SC}$ and untransduced H9 hESC cultures that were undifferentiated or at 7 days post-BMP4-induction. DNA was hybridized to an Infinium HumanMethylation450 BeadChip array (Illumina) using standard protocols. Methylation data were imported into the Illumina Genome Studio software and converted to a Partek project file (.ppj) with the Partek Methylation Module. This file contained the processed beta-values (quantitative methylation levels for each probe) and was imported into the Partek Genomics Suite software (Partek) using the Illumina Methylation Workflow tool. Data were log-transformed and analyzed using the Partek ANOVA tool to generate probe-level statistics that included *P*-value (*t*-test), *F*-value (signal-to-noise ratio), mean methylation levels and group methylation differences. These values were also determined for genomic regions by using the Partek's Region Detection tool with following parameters: minimum three consecutive probes with significance of $P < 0.01$, mean methylation difference of 0.2 (20%) and mean *F*-value across the region of $F = 50$. To identify methylation differences that were the result of *NLRP7* knockdown in differentiated and undifferentiated hESCs, above statistics were used to compare all six $shNLRP7^{KD}$ data sets (undifferentiated and differentiated combined) as the test group to all other samples (H9 hESCs and $shNLRP7^{SC}$) as the control group. Significant differences between groups meeting these criteria at the probe level are presented in Supplementary Material, Table S1, and the volcano plot in Figure 5A, and at the gene region level in Supplementary Material, Table S3. We also calculated descriptive statistics for probes with altered methylation in $shNLRP7^{KD}$ vis-à-vis CpG islands, gene bodies and intergenic regions (Supplementary Material, Table S2). Array-data analysis was repeated for differentiated and undifferentiated hESCs separately, but no regions met the above outlined significance criteria for DNA methylation level changes in $shNLRP7^{KD}$ compared with other hESCs (H9 hESCs and $shNLRP7^{SC}$). We used the Partek Genomics Suite software Genome Viewer Tool for all data visualizations.

Bisulfite sequencing

Bisulfite conversion was carried out on 1 μg of DNA from $shNLRP7^{KD}$, $shNLRP7^{SC}$ and untransduced undifferentiated and BMP4-differentiated H9 hESCs using the EZ DNA Methylation Kit (Zymo Research, D5001) or as previously described (45). Primers for the amplification of bisulfite-converted DNA were 5′-GGAGATTAAGAGTAGTAGGGGG-3′ and 5′-CCC AAAACTCTACAACCTTAAA-3′ for *SUCLG2*, 5′-GTAGTT AGTGAGTAAGGAGAG-3′ and 5′-AACCCCATAAAAATA CTTCCCT-3′ for *FBXO4*, 5′-AATTTTGGYGGAGTTGA TGGGTGGTTGTAG-3′ and 5′-ACTCCRACCTAATCCC AAAATAAAAACAC-3′ for *ZFP42*. Amplicons were cloned into pcDNA3.3 Topo TA vector (Invitrogen, K8300-01) and transformed into One Shot® Mach1™ T1 Phage-Resistant Chemically Competent *E. coli* (Invitrogen, C8620-03). Ten to 16 clones for each gene were sequenced in forward and reverse orientation at Beckman Coulter Genomics (Danvers, MA, USA). Electropherograms were analyzed using the Sequencher® version 5.1 software (Gene Codes Corporation).

Gene expression analysis by qRT-PCR

One microgram of total RNA was reverse-transcribed into cDNA using the qScript cDNA SuperMix (Quanta Biosciences). qRT-PCR was performed using PerfeCTa® SYBR® Green FastMix on the Applied Biosystems StepOnePlus Real-Time instrument. Analysis was by the $\Delta\Delta C_t$ method, with GAPDH as the housekeeping gene. Primer sequences for qRT-PCR are provided in the following table.

Gene	Forward primer	Reverse primer
GAPDH	5′-CTCCCGCTTCGCTCTCTG-3′	5′-AGTTAAAAGCAGCCCTGGTG-3′
NLRP7	5′-GGCCAGAATCATTTGTGGAA-3′	5′-TTTTCTTTCACTTCCTCCAACA-3′
NLRP2	5′-TCTGGACCTGGGTCAGAATC-3′	5′-CCAGCAGCTTATTGAGTTCAT-3′
POU5F1	5′-GCCGGTTACAGAACCACACT-3′	5′-AGTGAGAGGCAACCTGGAGA-3′
PAPPE	5′-CCAAGCCCACGAGTATCAAT-3′	5′-TCTGGGAGTCTTGTGGGTTC-3′
GCM1	5′-TGAGGGGAGTCGAATAGGTG-3′	5′-TAGGAATCTGGCCACTCCTG-3′
FBXO4	5′-GCATTTTTTGACTACATGGCA-3′	5′-CGGCTGGATTTTGAAGCTCT-3′
INSL4	5′-CCCATGCCTGAGAAGACATT-3′	5′-GTTGTTGGAGGTTGACACCA-3′
ZFP42	5′-GAGGCTGGAGCCTGTGTG-3′	5′-TGTGCCCTTCTTGAAGGTTT-3′
SUCGL2	5′-TGATGTCTGACAACGGAGTGA-3′	5′-GCTGTCCCACAACATTAGGG-3′

Statistical analysis

Unpaired Student's *t*-test was used for statistical analysis of RT-PCR results from ChIP and gene expression experiments, with $P < 0.05$ considered significant. Significance levels for each result are provided in the main text and figures where applicable. Statistical analysis for methylation array data is outlined above.

Accession numbers

The Illumina Infinium HumanMethylation450 BeadChip array data are available from the GEO database under accession number GSE45727.

AUTHORS' CONTRIBUTIONS

S.M. and S.W. designed and performed most of the experiments and data analysis, prepared figures and wrote initial drafts of the paper. H.-H.P. and S.O. performed initial experiments for NLRP7 interactor identification. B.S. performed the initial methylation array data analysis and presentation, Y.-W.W. and Z.L. analyzed methylation array data for overlap with YY1-binding sites. M.K. designed the *pSAM2 shNLRP7*^{KD} vector, generated knockdown ES cell lines and supervised M.I. and E.M.M., who constructed and confirmed the *shNLRP7*^{KD} vector. I.B.V. was responsible for project design, oversight of all experiments and interpretation, final manuscript and figure preparation.

SUPPLEMENTARY MATERIAL

Supplementary Material is available at *HMG* online.

ACKNOWLEDGEMENTS

We thank Dr M. Goodell for critical reading of the manuscript and Robert Milczawrek and the BCM Human ESC Core for help initiating the human ESC cell work. We also thank Vicky Brandt for editorial help.

Conflict of Interest statement. None declared.

FUNDING

This work was supported in part by NIH grants R21HD058081, R01HD045970, 5P01GM081627 and by grant 6250-51000-055 from the USDA/ARS to I.B.V. The project was also supported by the BCM IDDRC grant number 5P30HD024064 from the Eunice Kennedy Shriver National Institute of Child Health and Human Development and grant number C06RR029965 from the National Center for Research Resources. The content is solely the responsibility of the authors and does not necessarily represent the official views of the Eunice Kennedy Shriver National Institute of Child Health and Human Development or the National Institutes of Health.

REFERENCES

1. Murdoch, S., Djuric, U., Mazhar, B., Seoud, M., Khan, R., Kuick, R., Bagga, R., Kircheisen, R., Ao, A., Ratti, B. *et al.* (2006) Mutations in NALP7 cause recurrent hydatidiform moles and reproductive wastage in humans. *Nat. Genet.*, **38**, 300–302.
2. Kou, Y.C., Shao, L., Peng, H.H., Rosetta, R., del Gaudio, D., Wagner, A.F., Al-Hussaini, T.K. and Van den Veyver, I.B. (2008) A recurrent intragenic genomic duplication, other novel mutations in NLRP7 and imprinting defects in recurrent biparental hydatidiform moles. *Mol. Hum. Reprod.*, **14**, 33–40.
3. Dixon, P.H., Trongwongsa, P., Abu-Hayyah, S., Ng, S.H., Akbar, S.A., Khawaja, N.P., Seckl, M.J., Savage, P.M. and Fisher, R.A. (2012) Mutations in NLRP7 are associated with diploid biparental hydatidiform moles, but not androgenetic complete moles. *J. Med. Genet.*, **49**, 206–211.
4. Hayward, B.E., De Vos, M., Talati, N., Abdollahi, M.R., Taylor, G.R., Meyer, E., Williams, D., Maher, E.R., Setna, F., Nazir, K. *et al.* (2009) Genetic and epigenetic analysis of recurrent hydatidiform mole. *Hum. Mutat.*, **30**, E629–E639.
5. Judson, H., Hayward, B.E., Sheridan, E. and Bonthron, D.T. (2002) A global disorder of imprinting in the human female germ line. *Nature*, **416**, 539–542.
6. El-Maarri, O., Seoud, M., Coullin, P., Herbiniaux, U., Oldenburg, J., Rouleau, G. and Slim, R. (2003) Maternal alleles acquiring paternal methylation patterns in biparental complete hydatidiform moles. *Hum. Mol. Genet.*, **12**, 1405–1413.
7. Fisher, R.A., Hodges, M.D., Rees, H.C., Sebire, N.J., Seckl, M.J., Newlands, E.S., Genest, D.R. and Castrillon, D.H. (2002) The maternally transcribed gene p57(KIP2) (CDNK1C) is abnormally expressed in both androgenetic and biparental complete hydatidiform moles. *Hum. Mol. Genet.*, **11**, 3267–3272.
8. Djuric, U., El-Maarri, O., Lamb, B., Kuick, R., Seoud, M., Coullin, P., Oldenburg, J., Hanash, S. and Slim, R. (2006) Familial molar tissues due to mutations in the inflammatory gene, NALP7, have normal postzygotic DNA methylation. *Hum. Genet.*, **120**, 390–395.
9. El-Maarri, O., Seoud, M., Riviere, J.B., Oldenburg, J., Walter, J., Rouleau, G. and Slim, R. (2005) Patients with familial biparental hydatidiform moles have normal methylation at imprinted genes. *Eur. J. Hum. Genet.*, **13**, 486–490.
10. Jia, D., Jurkowska, R.Z., Zhang, X., Jeltsch, A. and Cheng, X. (2007) Structure of Dnmt3a bound to Dnmt3L suggests a model for de novo DNA methylation. *Nature*, **449**, 248–251.
11. Ciccone, D.N., Su, H., Hevi, S., Gay, F., Lei, H., Bajko, J., Xu, G., Li, E. and Chen, T. (2009) KDM1B is a histone H3K4 demethylase required to establish maternal genomic imprints. *Nature*, **461**, 415–418.

12. Chotalia, M., Smallwood, S.A., Ruf, N., Dawson, C., Lucifero, D., Frontera, M., James, K., Dean, W. and Kelsey, G. (2009) Transcription is required for establishment of germline methylation marks at imprinted genes. *Genes Dev.*, **23**, 105–117.
13. Blackledge, N.P., Zhou, J.C., Tolstorukov, M.Y., Farcas, A.M., Park, P.J. and Klose, R.J. (2010) Cpg islands recruit a histone H3 lysine 36 demethylase. *Mol. Cell*, **38**, 179–190.
14. Ting, J.P., Kastner, D.L. and Hoffman, H.M. (2006) CATERPILLERs, pyrin and hereditary immunological disorders. *Nat. Rev. Immunol.*, **6**, 183–195.
15. Tian, X., Pascal, G. and Monget, P. (2009) Evolution and functional divergence of NLRP genes in mammalian reproductive systems. *BMC Evol. Biol.*, **9**, 202.
16. Zhang, P., Dixon, M., Zucchelli, M., Hambiliki, F., Levkov, L., Hovatta, O. and Kere, J. (2008) Expression analysis of the NLRP gene family suggests a role in human preimplantation development. *PLoS One*, **3**, e2755.
17. El-Maarri, O. and Slim, R. (2006) Familial hydatidiform molar pregnancy: the germline imprinting defect hypothesis? *Curr. Top Microbiol. Immunol.*, **301**, 229–241.
18. Slim, R. and Mehio, A. (2007) The genetics of hydatidiform moles: new lights on an ancient disease. *Clin. Genet.*, **71**, 25–34.
19. Messaed, C., Akoury, E., Djuric, U., Zeng, J., Saleh, M., Gilbert, L., Seoud, M., Qureshi, S. and Slim, R. (2011) NLRP7, a nucleotide oligomerization domain-like receptor protein, is required for normal cytokine secretion and co-localizes with Golgi and the microtubule-organizing center. *J. Biol. Chem.*, **286**, 43313–43323.
20. Reddy, R., Akoury, E., Phuong Nguyen, N.M., Abdul-Rahman, O.A., Dery, C., Gupta, N., Daley, W.P., Ao, A., Landolsi, H., Ann Fisher, R. *et al.* (2012) Report of four new patients with protein-truncating mutations in C6orf221/KHDC3L and colocalization with NLRP7. *Eur. J. Hum. Genet.*, **21**, 957–964.
21. Meyer, E., Lim, D., Pasha, S., Tee, L.J., Rahman, F., Yates, J.R., Woods, C.G., Reik, W. and Maher, E.R. (2009) Germline mutation in NLRP2 (NALP2) in a familial imprinting disorder (Beckwith-Wiedemann Syndrome). *PLoS Genet.*, **5**, e1000423.
22. Andreasen, L., Bolund, L., Niemann, I., Hansen, E.S. and Sunde, L. (2012) Mosaic moles and non-familial biparental moles are not caused by mutations in NLRP7, NLRP2 or C6orf221. *Mol. Hum. Reprod.*, **18**, 593–598.
23. Okada, K., Hirota, E., Mizutani, Y., Fujioka, T., Shuin, T., Miki, T., Nakamura, Y. and Katagiri, T. (2004) Oncogenic role of NALP7 in testicular seminomas. *Cancer Sci.*, **95**, 949–954.
24. McDaniel, P. and Wu, X. (2009) Identification of oocyte-selective NLRP genes in rhesus macaque monkeys (*Macaca mulatta*). *Mol. Reprod. Dev.*, **76**, 151–159.
25. Kim, J. (2008) Multiple YY1 and CTCF binding sites in imprinting control regions. *Epigenetics*, **3**, 115–118.
26. Xu, R.H., Chen, X., Li, D.S., Li, R., Addicks, G.C., Glennon, C., Zwaka, T.P. and Thomson, J.A. (2002) BMP4 initiates human embryonic stem cell differentiation to trophoblast. *Nat. Biotechnol.*, **20**, 1261–1264.
27. Zhang, L., Magli, A., Catanese, J., Xu, Z., Kyba, M. and Perlingeiro, R.C. (2011) Modulation of TGF-beta signaling by endoglin in murine hemangioblast development and primitive hematopoiesis. *Blood*, **118**, 88–97.
28. Iacovino, M., Bosnakovski, D., Fey, H., Rux, D., Bajwa, G., Mahen, E., Mitanoska, A., Xu, Z. and Kyba, M. (2011) Inducible cassette exchange: a rapid and efficient system enabling conditional gene expression in embryonic stem and primary cells. *Stem Cells*, **29**, 1580–1588.
29. Sun, B., Ito, M., Mendjan, S., Ito, Y., Brons, I.G., Murrell, A., Vallier, L., Ferguson-Smith, A.C. and Pedersen, R.A. (2012) Status of genomic imprinting in epigenetically distinct pluripotent stem cells. *Stem Cells*, **30**, 161–168.
30. Rugg-Gunn, P.J., Ferguson-Smith, A.C. and Pedersen, R.A. (2007) Status of genomic imprinting in human embryonic stem cells as revealed by a large cohort of independently derived and maintained lines. *Hum. Mol. Genet.*, **16** (Spec No. 2), R243–R251.
31. Smallwood, S.A., Tomizawa, S., Krueger, F., Ruf, N., Carli, N., Segonds-Pichon, A., Sato, S., Hata, K., Andrews, S.R. and Kelsey, G. (2011) Dynamic CpG island methylation landscape in oocytes and preimplantation embryos. *Nat. Genet.*, **43**, 811–814.
32. Smallwood, S.A. and Kelsey, G. (2012) De novo DNA methylation: a germ cell perspective. *Trends Genet.*, **28**, 33–42.
33. Proudhon, C., Duffie, R., Ajjan, S., Cowley, M., Iranzo, J., Carbajosa, G., Saadeh, H., Holland, M.L., Oakey, R.J., Rakyan, V.K. *et al.* (2012) Protection against de novo methylation is instrumental in maintaining parent-of-origin methylation inherited from the gametes. *Mol. Cell*, **47**, 909–920.
34. Doi, A., Park, I.H., Wen, B., Murakami, P., Aryee, M.J., Irizarry, R., Herb, B., Ladd-Acosta, C., Rho, J., Loewer, S. *et al.* (2009) Differential methylation of tissue- and cancer-specific CpG island shores distinguishes human induced pluripotent stem cells, embryonic stem cells and fibroblasts. *Nat. Genet.*, **41**, 1350–1353.
35. Mongan, N.P., Martin, K.M. and Gudas, L.J. (2006) The putative human stem cell marker, Rex-1 (Zfp42): structural classification and expression in normal human epithelial and carcinoma cell cultures. *Mol. Carcinog.*, **45**, 887–900.
36. Ben-Shushan, E., Thompson, J.R., Gudas, L.J. and Bergman, Y. (1998) Rex-1, a gene encoding a transcription factor expressed in the early embryo, is regulated via Oct-3/4 and Oct-6 binding to an octamer site and a novel protein, Rox-1, binding to an adjacent site. *Mol. Cell. Biol.*, **18**, 1866–1878.
37. Shi, W., Wang, H., Pan, G., Geng, Y., Guo, Y. and Pei, D. (2006) Regulation of the pluripotency marker Rex-1 by Nanog and Sox2. *J. Biol. Chem.*, **281**, 23319–23325.
38. Kim, J.D., Kim, H., Ekram, M.B., Yu, S., Faulk, C. and Kim, J. (2011) Rex1/Zfp42 as an epigenetic regulator for genomic imprinting. *Hum. Mol. Genet.*, **20**, 1353–1362.
39. Khare, S., Dorfleutner, A., Bryan, N.B., Yun, C., Radian, A.D., de Almeida, L., Rojanasakul, Y. and Stehlik, C. (2012) An NLRP7-containing inflammasome mediates recognition of microbial lipopeptides in human macrophages. *Immunity*, **36**, 464–476.
40. Ogura, Y., Sutterwala, F.S. and Flavell, R.A. (2006) The inflammasome: first line of the immune response to cell stress. *Cell*, **126**, 659–662.
41. Sasaki, H. and Matsui, Y. (2008) Epigenetic events in mammalian germ-cell development: reprogramming and beyond. *Nat. Rev. Genet.*, **9**, 129–140.
42. Parry, D.A., Logan, C.V., Hayward, B.E., Shires, M., Landolsi, H., Diggle, C., Carr, I., Rittore, C., Touitou, I., Philibert, L. *et al.* (2011) Mutations causing familial biparental hydatidiform mole implicate c6orf221 as a possible regulator of genomic imprinting in the human oocyte. *Am. J. Hum. Genet.*, **89**, 451–458.
43. Schulz, L.C., Ezashi, T., Das, P., Westfall, S.D., Livingston, K.A. and Roberts, R.M. (2008) Human embryonic stem cells as models for trophoblast differentiation. *Placenta*, **29** (Suppl. A), S10–S16.
44. Rugg-Gunn, P.J., Ferguson-Smith, A.C. and Pedersen, R.A. (2005) Human embryonic stem cells as a model for studying epigenetic regulation during early development. *Cell Cycle*, **4**, 1323–1326.
45. Frommer, M., McDonald, L.E., Millar, D.S., Collis, C.M., Watt, F., Grigg, G.W., Molloy, P.L. and Paul, C.L. (1992) A genomic sequencing protocol that yields a positive display of 5-methylcytosine residues in individual DNA strands. *Proc. Natl Acad. Sci. USA*, **89**, 1827–1831.